Search for b→u transitions in B^{±}→[K^{#}π^{±}π^{0}]_{D}K^{±} decays

BABAR-PUB-11/006
SLAC-PUB-14444

Search for $b \to u$ Transitions in $B^{\pm} \to [K^{\mp}\pi^{\pm}\pi^{0}]_{D}K^{\pm}$ Decays

J. P. Lees,[1] V. Poireau,[1] V. Tisserand,[1] J. Garra Tico,[2] E. Grauges,[2] M. Martinelli[ab],[3] D. A. Milanes[a],[3] A. Palano[ab],[3] M. Pappagallo[ab],[3] G. Eigen,[4] B. Stugu,[4] L. Sun,[4] D. N. Brown,[5] L. T. Kerth,[5] Yu. G. Kolomensky,[5] G. Lynch,[5] H. Koch,[6] T. Schroeder,[6] D. J. Asgeirsson,[7] C. Hearty,[7] T. S. Mattison,[7] J. A. McKenna,[7] A. Khan,[8] V. E. Blinov,[9] A. R. Buzykaev,[9] V. P. Druzhinin,[9] V. B. Golubev,[9] E. A. Kravchenko,[9] A. P. Onuchin,[9] S. I. Serednyakov,[9] Yu. I. Skovpen,[9] E. P. Solodov,[9] K. Yu. Todyshev,[9] A. N. Yushkov,[9] M. Bondioli,[10] S. Curry,[10] D. Kirkby,[10] A. J. Lankford,[10] M. Mandelkern,[10] D. P. Stoker,[10] H. Atmacan,[11] J. W. Gary,[11] F. Liu,[11] O. Long,[11] G. M. Vitug,[11] C. Campagnari,[12] T. M. Hong,[12] D. Kovalskyi,[12] J. D. Richman,[12] C. A. West,[12] A. M. Eisner,[13] J. Kroseberg,[13] W. S. Lockman,[13] A. J. Martinez,[13] T. Schalk,[13] B. A. Schumm,[13] A. Seiden,[13] C. H. Cheng,[14] D. A. Doll,[14] B. Echenard,[14] K. T. Flood,[14] D. G. Hitlin,[14] P. Ongmongkolkul,[14] F. C. Porter,[14] A. Y. Rakitin,[14] R. Andreassen,[15] M. S. Dubrovin,[15] B. T. Meadows,[15] M. D. Sokoloff,[15] P. C. Bloom,[16] W. T. Ford,[16] A. Gaz,[16] M. Nagel,[16] U. Nauenberg,[16] J. G. Smith,[16] S. R. Wagner,[16] R. Ayad,[17,*] W. H. Toki,[17] B. Spaan,[18] M. J. Kobel,[19] K. R. Schubert,[19] R. Schwierz,[19] D. Bernard,[20] M. Verderi,[20] P. J. Clark,[21] S. Playfer,[21] J. E. Watson,[21] D. Bettoni[a],[22] C. Bozzi[a],[22] R. Calabrese[ab],[22] G. Cibinetto[ab],[22] E. Fioravanti[ab],[22] I. Garzia[ab],[22] E. Luppi[ab],[22] M. Munerato[ab],[22] M. Negrini[ab],[22] L. Piemontese[a],[22] R. Baldini-Ferroli,[23] A. Calcaterra,[23] R. de Sangro,[23] G. Finocchiaro,[23] M. Nicolaci,[23] S. Pacetti,[23] P. Patteri,[23] I. M. Peruzzi,[23,†] M. Piccolo,[23] M. Rama,[23] A. Zallo,[23] R. Contri[ab],[24] E. Guido[ab],[24] M. Lo Vetere[ab],[24] M. R. Monge[ab],[24] S. Passaggio[a],[24] C. Patrignani[ab],[24] E. Robutti[a],[24] B. Bhuyan,[25] V. Prasad,[25] C. L. Lee,[26] M. Morii,[26] A. J. Edwards,[27] A. Adametz,[28] J. Marks,[28] U. Uwer,[28] F. U. Bernlochner,[29] M. Ebert,[29] H. M. Lacker,[29] T. Lueck,[29] P. D. Dauncey,[30] M. Tibbetts,[30] P. K. Behera,[31] U. Mallik,[31] C. Chen,[32] J. Cochran,[32] H. B. Crawley,[32] W. T. Meyer,[32] S. Prell,[32] E. I. Rosenberg,[32] A. E. Rubin,[32] A. V. Gritsan,[33] Z. J. Guo,[33] N. Arnaud,[34] M. Davier,[34] D. Derkach,[34] G. Grosdidier,[34] F. Le Diberder,[34] A. M. Lutz,[34] B. Malaescu,[34] P. Roudeau,[34] M. H. Schune,[34] A. Stocchi,[34] G. Wormser,[34] D. J. Lange,[35] D. M. Wright,[35] I. Bingham,[36] C. A. Chavez,[36] J. P. Coleman,[36] J. R. Fry,[36] E. Gabathuler,[36] D. E. Hutchcroft,[36] D. J. Payne,[36] C. Touramanis,[36] A. J. Bevan,[37] F. Di Lodovico,[37] R. Sacco,[37] M. Sigamani,[37] G. Cowan,[38] S. Paramesvaran,[38] D. N. Brown,[39] C. L. Davis,[39] A. G. Denig,[40] M. Fritsch,[40] W. Gradl,[40] A. Hafner,[40] E. Prencipe,[40] K. E. Alwyn,[41] D. Bailey,[41] R. J. Barlow,[41] G. Jackson,[41] G. D. Lafferty,[41] R. Cenci,[42] B. Hamilton,[42] A. Jawahery,[42] D. A. Roberts,[42] G. Simi,[42] C. Dallapiccola,[43] R. Cowan,[44] D. Dujmic,[44] G. Sciolla,[44] D. Lindemann,[45] P. M. Patel,[45] S. H. Robertson,[45] M. Schram,[45] P. Biassoni[ab],[46] A. Lazzaro[ab],[46] V. Lombardo[a],[46] F. Palombo[ab],[46] S. Stracka[ab],[46] L. Cremaldi,[47] R. Godang,[47,‡] R. Kroeger,[47] P. Sonnek,[47] D. J. Summers,[47] X. Nguyen,[48] P. Taras,[48] G. De Nardo[ab],[49] D. Monorchio[ab],[49] G. Onorato[ab],[49] C. Sciacca[ab],[49] G. Raven,[50] H. L. Snoek,[50] C. P. Jessop,[51] K. J. Knoepfel,[51] J. M. LoSecco,[51] W. F. Wang,[51] K. Honscheid,[52] R. Kass,[52] J. Brau,[53] R. Frey,[53] N. B. Sinev,[53] D. Strom,[53] E. Torrence,[53] E. Feltresi[ab],[54] N. Gagliardi[ab],[54] M. Margoni[ab],[54] M. Morandin[a],[54] M. Posocco[a],[54] M. Rotondo[a],[54] F. Simonetto[ab],[54] R. Stroili[ab],[54] E. Ben-Haim,[55] M. Bomben,[55] G. R. Bonneaud,[55] H. Briand,[55] G. Calderini,[55] J. Chauveau,[55] O. Hamon,[55] Ph. Leruste,[55] G. Marchiori,[55] J. Ocariz,[55] S. Sitt,[55] M. Biasini[ab],[56] E. Manoni[ab],[56] A. Rossi[ab],[56] C. Angelini[ab],[57] G. Batignani[ab],[57] S. Bettarini[ab],[57] M. Carpinelli[ab],[57,§] G. Casarosa[ab],[57] A. Cervelli[ab],[57] F. Forti[ab],[57] M. A. Giorgi[ab],[57] A. Lusiani[ac],[57] N. Neri[ab],[57] B. Oberhof[ab],[57] E. Paoloni[ab],[57] A. Perez[a],[57] G. Rizzo[ab],[57] J. J. Walsh[a],[57] D. Lopes Pegna,[58] C. Lu,[58] J. Olsen,[58] A. J. S. Smith,[58] A. V. Telnov,[58] F. Anulli[a],[59] G. Cavoto[a],[59] R. Faccini[ab],[59] F. Ferrarotto[a],[59] F. Ferroni[ab],[59] M. Gaspero[ab],[59] L. Li Gioi[a],[59] M. A. Mazzoni[a],[59] G. Piredda[a],[59] C. Buenger,[60] T. Hartmann,[60] T. Leddig,[60] H. Schröder,[60] R. Waldi,[60] T. Adye,[61] E. O. Olaiya,[61] F. F. Wilson,[61] S. Emery,[62] G. Hamel de Monchenault,[62] G. Vasseur,[62] Ch. Yèche,[62] D. Aston,[63] D. J. Bard,[63] R. Bartoldus,[63] J. F. Benitez,[63] C. Cartaro,[63] M. R. Convery,[63] J. Dorfan,[63] G. P. Dubois-Felsmann,[63] W. Dunwoodie,[63] R. C. Field,[63] M. Franco Sevilla,[63] B. G. Fulsom,[63] A. M. Gabareen,[63] M. T. Graham,[63] P. Grenier,[63] C. Hast,[63] W. R. Innes,[63] M. H. Kelsey,[63] H. Kim,[63] P. Kim,[63] M. L. Kocian,[63] D. W. G. S. Leith,[63] P. Lewis,[63] S. Li,[63] B. Lindquist,[63] S. Luitz,[63] V. Luth,[63] H. L. Lynch,[63] D. B. MacFarlane,[63] D. R. Muller,[63] H. Neal,[63] S. Nelson,[63] I. Ofte,[63] M. Perl,[63] T. Pulliam,[63] B. N. Ratcliff,[63] A. Roodman,[63] A. A. Salnikov,[63] V. Santoro,[63] R. H. Schindler,[63] A. Snyder,[63] D. Su,[63] M. K. Sullivan,[63] J. Va'vra,[63] A. P. Wagner,[63] M. Weaver,[63] W. J. Wisniewski,[63] M. Wittgen,[63] D. H. Wright,[63] H. W. Wulsin,[63] A. K. Yarritu,[63] C. C. Young,[63] V. Ziegler,[63] W. Park,[64] M. V. Purohit,[64] R. M. White,[64] J. R. Wilson,[64] A. Randle-Conde,[65] S. J. Sekula,[65] M. Bellis,[66] P. R. Burchat,[66] T. S. Miyashita,[66] M. S. Alam,[67] J. A. Ernst,[67] R. Gorodeisky,[68]

N. Guttman,[68] D. R. Peimer,[68] A. Soffer,[68] P. Lund,[69] S. M. Spanier,[69] R. Eckmann,[70] J. L. Ritchie,[70] A. M. Ruland,[70] C. J. Schilling,[70] R. F. Schwitters,[70] B. C. Wray,[70] J. M. Izen,[71] X. C. Lou,[71] F. Bianchi[ab],[72] D. Gamba[ab],[72] L. Lanceri[ab],[73] L. Vitale[ab],[73] N. Lopez-March,[74] F. Martinez-Vidal,[74] A. Oyanguren,[74] H. Ahmed,[75] J. Albert,[75] Sw. Banerjee,[75] H. H. F. Choi,[75] G. J. King,[75] R. Kowalewski,[75] M. J. Lewczuk,[75] C. Lindsay,[75] I. M. Nugent,[75] J. M. Roney,[75] R. J. Sobie,[75] T. J. Gershon,[76] P. F. Harrison,[76] T. E. Latham,[76] E. M. T. Puccio,[76] H. R. Band,[77] S. Dasu,[77] Y. Pan,[77] R. Prepost,[77] C. O. Vuosalo,[77] and S. L. Wu[77]

(The *BABAR* Collaboration)

[1]*Laboratoire d'Annecy-le-Vieux de Physique des Particules (LAPP), Université de Savoie, CNRS/IN2P3, F-74941 Annecy-Le-Vieux, France*
[2]*Universitat de Barcelona, Facultat de Fisica, Departament ECM, E-08028 Barcelona, Spain*
[3]*INFN Sezione di Bari[a]; Dipartimento di Fisica, Università di Bari[b], I-70126 Bari, Italy*
[4]*University of Bergen, Institute of Physics, N-5007 Bergen, Norway*
[5]*Lawrence Berkeley National Laboratory and University of California, Berkeley, California 94720, USA*
[6]*Ruhr Universität Bochum, Institut für Experimentalphysik 1, D-44780 Bochum, Germany*
[7]*University of British Columbia, Vancouver, British Columbia, Canada V6T 1Z1*
[8]*Brunel University, Uxbridge, Middlesex UB8 3PH, United Kingdom*
[9]*Budker Institute of Nuclear Physics, Novosibirsk 630090, Russia*
[10]*University of California at Irvine, Irvine, California 92697, USA*
[11]*University of California at Riverside, Riverside, California 92521, USA*
[12]*University of California at Santa Barbara, Santa Barbara, California 93106, USA*
[13]*University of California at Santa Cruz, Institute for Particle Physics, Santa Cruz, California 95064, USA*
[14]*California Institute of Technology, Pasadena, California 91125, USA*
[15]*University of Cincinnati, Cincinnati, Ohio 45221, USA*
[16]*University of Colorado, Boulder, Colorado 80309, USA*
[17]*Colorado State University, Fort Collins, Colorado 80523, USA*
[18]*Technische Universität Dortmund, Fakultät Physik, D-44221 Dortmund, Germany*
[19]*Technische Universität Dresden, Institut für Kern- und Teilchenphysik, D-01062 Dresden, Germany*
[20]*Laboratoire Leprince-Ringuet, Ecole Polytechnique, CNRS/IN2P3, F-91128 Palaiseau, France*
[21]*University of Edinburgh, Edinburgh EH9 3JZ, United Kingdom*
[22]*INFN Sezione di Ferrara[a]; Dipartimento di Fisica, Università di Ferrara[b], I-44100 Ferrara, Italy*
[23]*INFN Laboratori Nazionali di Frascati, I-00044 Frascati, Italy*
[24]*INFN Sezione di Genova[a]; Dipartimento di Fisica, Università di Genova[b], I-16146 Genova, Italy*
[25]*Indian Institute of Technology Guwahati, Guwahati, Assam, 781 039, India*
[26]*Harvard University, Cambridge, Massachusetts 02138, USA*
[27]*Harvey Mudd College, Claremont, California 91711*
[28]*Universität Heidelberg, Physikalisches Institut, Philosophenweg 12, D-69120 Heidelberg, Germany*
[29]*Humboldt-Universität zu Berlin, Institut für Physik, Newtonstr. 15, D-12489 Berlin, Germany*
[30]*Imperial College London, London, SW7 2AZ, United Kingdom*
[31]*University of Iowa, Iowa City, Iowa 52242, USA*
[32]*Iowa State University, Ames, Iowa 50011-3160, USA*
[33]*Johns Hopkins University, Baltimore, Maryland 21218, USA*
[34]*Laboratoire de l'Accélérateur Linéaire, IN2P3/CNRS et Université Paris-Sud 11, Centre Scientifique d'Orsay, B. P. 34, F-91898 Orsay Cedex, France*
[35]*Lawrence Livermore National Laboratory, Livermore, California 94550, USA*
[36]*University of Liverpool, Liverpool L69 7ZE, United Kingdom*
[37]*Queen Mary, University of London, London, E1 4NS, United Kingdom*
[38]*University of London, Royal Holloway and Bedford New College, Egham, Surrey TW20 0EX, United Kingdom*
[39]*University of Louisville, Louisville, Kentucky 40292, USA*
[40]*Johannes Gutenberg-Universität Mainz, Institut für Kernphysik, D-55099 Mainz, Germany*
[41]*University of Manchester, Manchester M13 9PL, United Kingdom*
[42]*University of Maryland, College Park, Maryland 20742, USA*
[43]*University of Massachusetts, Amherst, Massachusetts 01003, USA*
[44]*Massachusetts Institute of Technology, Laboratory for Nuclear Science, Cambridge, Massachusetts 02139, USA*
[45]*McGill University, Montréal, Québec, Canada H3A 2T8*
[46]*INFN Sezione di Milano[a]; Dipartimento di Fisica, Università di Milano[b], I-20133 Milano, Italy*
[47]*University of Mississippi, University, Mississippi 38677, USA*
[48]*Université de Montréal, Physique des Particules, Montréal, Québec, Canada H3C 3J7*
[49]*INFN Sezione di Napoli[a]; Dipartimento di Scienze Fisiche, Università di Napoli Federico II[b], I-80126 Napoli, Italy*
[50]*NIKHEF, National Institute for Nuclear Physics and High Energy Physics, NL-1009 DB Amsterdam, The Netherlands*
[51]*University of Notre Dame, Notre Dame, Indiana 46556, USA*
[52]*Ohio State University, Columbus, Ohio 43210, USA*

[53]University of Oregon, Eugene, Oregon 97403, USA
[54]INFN Sezione di Padova[a]; Dipartimento di Fisica, Università di Padova[b], I-35131 Padova, Italy
[55]Laboratoire de Physique Nucléaire et de Hautes Energies,
IN2P3/CNRS, Université Pierre et Marie Curie-Paris6,
Université Denis Diderot-Paris7, F-75252 Paris, France
[56]INFN Sezione di Perugia[a]; Dipartimento di Fisica, Università di Perugia[b], I-06100 Perugia, Italy
[57]INFN Sezione di Pisa[a]; Dipartimento di Fisica,
Università di Pisa[b]; Scuola Normale Superiore di Pisa[c], I-56127 Pisa, Italy
[58]Princeton University, Princeton, New Jersey 08544, USA
[59]INFN Sezione di Roma[a]; Dipartimento di Fisica,
Università di Roma La Sapienza[b], I-00185 Roma, Italy
[60]Universität Rostock, D-18051 Rostock, Germany
[61]Rutherford Appleton Laboratory, Chilton, Didcot, Oxon, OX11 0QX, United Kingdom
[62]CEA, Irfu, SPP, Centre de Saclay, F-91191 Gif-sur-Yvette, France
[63]SLAC National Accelerator Laboratory, Stanford, California 94309 USA
[64]University of South Carolina, Columbia, South Carolina 29208, USA
[65]Southern Methodist University, Dallas, Texas 75275, USA
[66]Stanford University, Stanford, California 94305-4060, USA
[67]State University of New York, Albany, New York 12222, USA
[68]Tel Aviv University, School of Physics and Astronomy, Tel Aviv, 69978, Israel
[69]University of Tennessee, Knoxville, Tennessee 37996, USA
[70]University of Texas at Austin, Austin, Texas 78712, USA
[71]University of Texas at Dallas, Richardson, Texas 75083, USA
[72]INFN Sezione di Torino[a]; Dipartimento di Fisica Sperimentale, Università di Torino[b], I-10125 Torino, Italy
[73]INFN Sezione di Trieste[a]; Dipartimento di Fisica, Università di Trieste[b], I-34127 Trieste, Italy
[74]IFIC, Universitat de Valencia-CSIC, E-46071 Valencia, Spain
[75]University of Victoria, Victoria, British Columbia, Canada V8W 3P6
[76]Department of Physics, University of Warwick, Coventry CV4 7AL, United Kingdom
[77]University of Wisconsin, Madison, Wisconsin 53706, USA

We present a study of the decays $B^\pm \to DK^\pm$ with D mesons reconstructed in the $K^+\pi^-\pi^0$ or $K^-\pi^+\pi^0$ final states, where D indicates a D^0 or a $\overline{D}^0$ meson. Using a sample of 474 million $B\overline{B}$ pairs collected with the *BABAR* detector at the PEP-II asymmetric-energy e^+e^- collider at SLAC, we measure the ratios $R^\pm \equiv \frac{\Gamma(B^\pm\to[K^\mp\pi^\pm\pi^0]_D K^\pm)}{\Gamma(B^\pm\to[K^\pm\pi^\mp\pi^0]_D K^\pm)}$. We obtain $R^+ = \left(5^{+12}_{-10}(\mathrm{stat})^{+2}_{-4}(\mathrm{syst})\right)\times 10^{-3}$ and $R^- = \left(12^{+12}_{-10}(\mathrm{stat})^{+3}_{-5}(\mathrm{syst})\right)\times 10^{-3}$, from which we extract the upper limits at 90% probability: $R^+ < 23\times 10^{-3}$ and $R^- < 29\times 10^{-3}$. Using these measurements, we obtain an upper limit for the ratio r_B of the magnitudes of the $b\to u$ and $b\to c$ amplitudes $r_B < 0.13$ at 90% probability.

PACS numbers: 13.25.Hw, 14.40.Nd

I. INTRODUCTION

CP violation effects are described in the Standard Model (SM) of elementary particles with a single phase in the Cabibbo-Kobayashi-Maskawa (CKM) quark mixing matrix V_{ij} [1]. One of the unitarity conditions for this matrix can be interpreted as a triangle in the plane of Wolfenstein parameters [2], where one of the angles is $\gamma = \arg\{-V^*_{ub}V_{ud}/V^*_{cb}V_{cd}\}$. Various methods to determine γ using $B^+ \to DK^+$ decays have been proposed [3–5]. In this paper, we consider the decay channel $B^+ \to DK^+$ with $D \to K^-\pi^+\pi^0$ [6] studied through the Atwood-Dunietz-Soni (ADS) method [4]. In this method the final state under consideration can be reached through $b\to c$ and $b\to u$ processes as indicated in Fig. 1 that are followed by either Cabibbo-favored or Cabibbo suppressed D^0 decays. The interplay between different decay channels leads to a possibility to extract the angle γ alongside with other parameters for these decays.

Following the ADS method, we search for $B^+ \to [K^-\pi^+\pi^0]_D K^+$ events, where the favored $B^+ \to \overline{D}^0 K^+$ decay, followed by the doubly- Cabibbo-suppressed $\overline{D}^0 \to K^-\pi^+\pi^0$ decay, interferes with the suppressed $B^+ \to D^0K^+$ decay, followed by the Cabibbo-favored $D^0 \to K^-\pi^+\pi^0$ decay. These are called "opposite-sign" events because the two kaons in the final state have opposite charges. We also reconstruct a larger sample of "same-sign" events, which mainly arise from the favored $B^+ \to \overline{D}^0 K^+$ decays followed by the Cabibbo-favored $\overline{D}^0 \to K^+\pi^-\pi^0$ decays. We define $f \equiv K^+\pi^-\pi^0$ and

*Now at Temple University, Philadelphia, Pennsylvania 19122, USA
†Also with Università di Perugia, Dipartimento di Fisica, Perugia, Italy
‡Now at University of South Alabama, Mobile, Alabama 36688, USA
§Also with Università di Sassari, Sassari, Italy

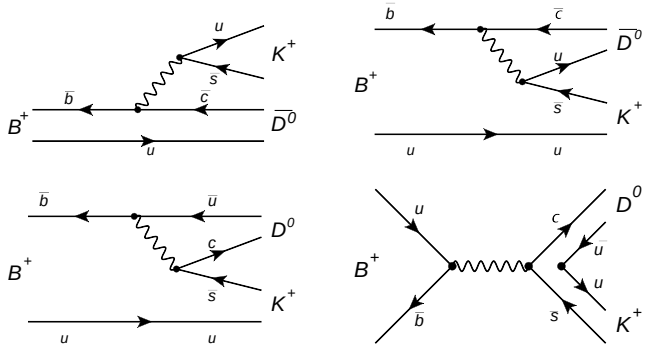

FIG. 1: Feynman diagrams for $B^+ \to \overline{D}^0 K^+$ (top, $\overline{b} \to \overline{c}$ transition) and $B^+ \to D^0 K^+$ (bottom, $\overline{b} \to \overline{u}$ transition).

$\bar{f} \equiv K^-\pi^+\pi^0$. We extract

$$R^+ = \frac{\Gamma(B^+ \to [\bar{f}]_D K^+)}{\Gamma(B^+ \to [f]_D K^+)}, \quad (1)$$

$$R^- = \frac{\Gamma(B^- \to [f]_D K^-)}{\Gamma(B^- \to [\bar{f}]_D K^-)}. \quad (2)$$

from the selected B^+ and B^- samples, respectively.

While our previous analysis [7] used another set of observables:

$$R_{\rm ADS} \equiv \frac{\Gamma(B^+ \to [\bar{f}]_D K^+) + \Gamma(B^- \to [f]_D K^-)}{\Gamma(B^+ \to [f]_D K^+) + \Gamma(B^- \to [\bar{f}]_D K^-)}, \quad (3)$$

$$A_{\rm ADS} \equiv \frac{\Gamma(B^- \to [f]_D K^-) - \Gamma(B^+ \to [\bar{f}]_D K^+)}{\Gamma(B^+ \to [\bar{f}]_D K^+) + \Gamma(B^- \to [f]_D K^-)}, \quad (4)$$

we prefer to use observables defined in Eqs. 1 and 2 since their statistical uncertainties, which dominate in the final error of this measurement, are uncorrelated.

The amplitude of the two-body B decay can be written as

$$A(B^+ \to D^0 K^+) = |A(B^+ \to \overline{D}^0 K^+)| r_B e^{i\gamma} e^{i\delta_B}, \quad (5)$$

where $r_B \equiv \frac{|A(B^+ \to D^0 K^+)|}{|A(B^+ \to \overline{D}^0 K^+)|}$ is the ratio of the magnitudes of the $b \to u$ and $b \to c$ amplitudes, δ_B is the CP conserving strong phase, and γ is the CP violating weak phase. For the three-body D decay we use similarly defined variables:

$$r_D^2 \equiv \frac{\Gamma\left(D^0 \to f\right)}{\Gamma\left(D^0 \to \bar{f}\right)} = \frac{\int d\vec{m}\, A_{\rm DCS}^2(\vec{m})}{\int d\vec{m}\, A_{\rm CF}^2(\vec{m})}, \quad (6)$$

$$k_D e^{i\delta_D} \equiv \frac{\int d\vec{m}\, A_{\rm DCS}(\vec{m}) A_{\rm CF}(\vec{m}) e^{i\delta(\vec{m})}}{\sqrt{\int d\vec{m}\, A_{\rm DCS}^2(\vec{m}) \int d\vec{m}\, A_{\rm CF}^2(\vec{m})}}, \quad (7)$$

where $A_{\rm CF}(\vec{m})$ and $A_{\rm DCS}(\vec{m})$ are the magnitude of the Cabibbo-favored and doubly-Cabibbo-Suppressed amplitudes, respectively, $\delta(\vec{m})$ is the relative strong phase, and $\vec{m}$ indicates a position in the D Dalitz plot of squared invariant masses $[m^2_{K\pi}, m^2_{K\pi^0}]$. The parameter k_D, called the coherence factor, can take values in the interval $[0, 1]$.

Neglecting D-mixing effects, which in the SM give negligible corrections to γ and do not affect the r_B measurement, the ratios R^+ and R^- are related to the B- and D-mesons' decay parameters through the following relations:

$$R^+ = r_B^2 + r_D^2 + 2 r_B r_D k_D \cos(\gamma + \delta), \quad (8)$$

$$R^- = r_B^2 + r_D^2 + 2 r_B r_D k_D \cos(\gamma - \delta), \quad (9)$$

with $\delta = \delta_B + \delta_D$. The values of k_D and δ_D measured by the CLEO-c collaboration [8], $k_D = 0.84 \pm 0.07$ and $\delta_D = (47^{+14}_{-17})^\circ$, are used in the signal yield estimation and r_B extraction. The ratio r_D has been measured in different experiments and we take the average value $r_D^2 = (2.2 \pm 0.1) \times 10^{-3}$ [9]. Its value is small compared to the present determination of r_B, which is taken to be (0.106 ± 0.016) [10]. According to Eqs. 8 and 9, this implies that the measurements of ratios $R^\pm$ is mainly sensitive to r_B. For the same reason, the sensitivity to γ is reduced, and therefore the main aim of this analysis is to measure R^+, R^-, and r_B. The current high precision on r_B is based on several earlier analyses by the *BABAR* [7, 11–13], BELLE [14–16], and CDF [17] collaborations.

This paper is an update of our previous analysis [7] based on 226×10^6 $B\overline{B}$ pairs and resulting in a measurement of $R_{\rm ADS} = (13^{+12}_{-10}) \times 10^{-3}$, which was translated into the 95% confidence level limit $r_B < 0.19$.

The results presented in this paper are obtained with 431 fb^{-1} of data collected at the $\Upsilon(4S)$ resonance with the *BABAR* detector at the PEP-II e^+e^- collider at SLAC, corresponding to 474×10^6 $B\overline{B}$ pairs. An additional "off-resonance" data sample of 45 fb^{-1}, collected at a center-of-mass (CM) energy 40 MeV below the $\Upsilon(4S)$ resonance, is used to study backgrounds from "continuum" events, $e^+e^- \to q\bar{q}$ ($q = u, d, s,$ or c).

II. EVENT RECONSTRUCTION AND SELECTION

The *BABAR* detector is described in detail elsewhere [18]. Charged-particle tracking is performed by a five-layer silicon vertex tracker (SVT) and a 40-layer drift chamber (DCH). In addition to providing precise position information for tracking, the SVT and DCH measure the specific ionization, which is used for identification of low-momentum charged particles. At higher momenta pions and kaons are distinguished by Cherenkov radiation detected in a ring-imaging device (DIRC). The positions and energies of photons are measured with an electromagnetic calorimeter (EMC) consisting of 6580 thallium-doped CsI crystals. These systems are mounted inside a 1.5 T solenoidal superconducting magnet. Muons are identified by the instrumented flux return, which is located outside the magnet.

The event selection is based on studies of off-resonance data and Monte Carlo (MC) simulations of continuum and $e^+e^- \to \Upsilon(4S) \to B\overline{B}$ events. The *BABAR* detector response is modeled with GEANT4 [19]. We also use

EvtGen [20] to model the kinematics of B meson decays and JetSet [21] to model continuum background processes. All selection criteria are optimized by maximizing the $S/\sqrt{S+B}$ ratio, where S and B are the expected numbers of the opposite-sign signal and background events, respectively. In the optimization we assume an opposite-sign branching fraction of 4×10^{-6} [9].

The charged kaon and pion identification criteria are based on a likelihood technique. These criteria are typically 85% efficient, depending on the momentum and polar angle, with misidentification rates at the 2% level. The π^0 candidates are reconstructed from pairs of photon candidates with an invariant mass in the interval $[119, 146]$ MeV/c^2 and with total energy greater than 200 MeV. Each photon should have energy greater than 70 MeV.

The neutral D meson candidates are reconstructed from a charged kaon, a charged pion, and a neutral pion. The correlation between the tails in the distribution of the $K\pi\pi^0$ invariant mass, m_D, and the π^0 candidate mass, m_{π^0}, is taken into account by requiring $|m_D - m_{\pi^0}|$ to be within 24 MeV/c^2 of its nominal value [9], which is 1.5 times the experimental resolution.

The B^+ candidates are reconstructed by combining D and K^+ candidates, and constraining them to originate from a common vertex. The probability distribution of the cosine of the B polar angle with respect to the beam axis in the CM frame, $\cos\theta_B$, is expected to be proportional to $(1-\cos^2\theta_B)$. We require $|\cos\theta_B| < 0.8$.

We measure two almost independent kinematic variables: the beam-energy substituted mass $m_{\rm ES} \equiv \sqrt{(s/2+\vec{p}_0\cdot\vec{p}_B)^2/E_0^2 - p_B^2}$, and the energy difference $\Delta E \equiv E_B - \sqrt{s}/2$, where E and $\vec{p}$ are the energy and momentum, the subscripts B and 0 refer to the candidate B meson and e^+e^- system, respectively, $\sqrt{s}$ is the center-of-mass energy, and E_B is measured in the CM frame. For correctly reconstructed B mesons the distribution of $m_{\rm ES}$ peaks at the B mass, and the distribution of ΔE peaks at zero. The B candidates are required to have ΔE in the range $[-23, 23]$ MeV (±1.3 standard deviations). We consider only events with $m_{\rm ES}$ in the range $[5.20, 5.29]$ GeV/c^2.

In less than 2% of the events, multiple B^+ candidates are present, and in these cases we choose that with a reconstructed D mass closest to the nominal mass value [9]. If more than one B^+ candidate share the same D candidate, we select that with the smallest $|\Delta E|$. In the following we refer to the selected candidate as $B_{\rm sig}$. All charged and neutral reconstructed particles not associated with $B_{\rm sig}$, but with the other B decay in the event, $B_{\rm other}$, are called the rest of the event.

III. BACKGROUND CHARACTERIZATION

After applying the selection criteria described above, the remaining background is composed of non-signal $B\overline{B}$ events and continuum events. Continuum background events, in contrast to $B\overline{B}$ events, are characterized by a jet-like topology. This difference can be exploited to discriminate between the two categories of events by means of a Fisher discriminant $\mathcal{F}$, which is a linear combination of six variables. The coefficients of the linear combination are chosen to maximize the separation between signal and continuum background so that $\mathcal{F}$ peaks at 1 for signal and at -1 for continuum background. They are determined with samples of simulated signal and continuum events, and validated using off-resonance data. In the Fisher discriminant we use the absolute value of the cosine of the angle between $B_{\rm sig}$ and $B_{\rm other}$ thrust axes, where the thrust axis is defined as the direction maximizing the sum of the longitudinal momenta of all the particles. Other variables included in $\mathcal{F}$ are the event shape moments $L_0 = \sum_i p_i$, and $L_2 = \sum_i p_i|\cos\theta_i|^2$, where the index i runs over all tracks and energy deposits in the rest of the event; p_i is the momentum; and θ_i is the angle with respect to the thrust axis of the $B_{\rm sig}$. These three variables are calculated in the CM system. We also use the distance between the decay vertices of $B_{\rm sig}$ and D, the distance of closest approach between K meson tracks belonging to signal decay chain, and $|\Delta t|$, the absolute value of the proper time interval between the $B_{\rm sig}$ and $B_{\rm other}$ decays [22]. The latter is calculated using the measured separation along the beam direction between the decay points of $B_{\rm sig}$ and $B_{\rm other}$ and the Lorentz boost of the CM frame. The $B_{\rm other}$ decay point is obtained from tracks that do not belong to the reconstructed $B_{\rm sig}$, with constraints from the $B_{\rm sig}$ momentum and the beam-spot location. We use $m_{\rm ES}$ and $\mathcal{F}$ to define two regions: the fit region, defined as $5.20 < m_{\rm ES} < 5.29\,{\rm GeV}/c^2$ and $-5 < \mathcal{F} < 5$, and the signal region, defined as $5.27 < m_{\rm ES} < 5.29$ GeV/c^2 and $0 < \mathcal{F} < 5$.

The $B\overline{B}$ background is divided into two components: non-peaking (combinatorial) and peaking. The latter consists of B-meson decays that have a well-pronounced peak in the $m_{\rm ES}$ signal region. One of the decay channels which can mimic opposite-sign signal events, is the $B^+ \to D\rho^+$ decay with $D \to K^+K^-$ and $\rho^+ \to \pi^+\pi^0$. In order to reduce this contribution, we veto events for which the invariant K^+K^- pair mass $m_{K^+K^-}$ is $|m_{K^+K^-} - M_{D({\rm PDG})}| > 20$ MeV/c^2 (with the D meson invariant mass, $M_{D({\rm PDG})}$, taken to be 1864.83 MeV/c^2 [9]). Simulations indicate that the remaining background is negligible.

Another possible source of peaking $B\overline{B}$ background is the decay $B^+ \to D\pi^+$ with $D \to K^+\pi^-\pi^0$, which can contribute to the signal region of the same-sign sample due to the misidentification of the π^+ as a K^+. The number of events is expected to be about 8% of the total same-sign signal sample (see Table I).

The charmless $B^+ \to K^+K^-\pi^+\pi^0$ decay can also contribute to the signal region. The branching fraction of this decay has not been measured. Therefore the size of this background is estimated from the sidebands of the reconstructed D mass, $1.904 < M_D < 2.000$ GeV/c^2 or

$1.700 < M_D < 1.824$ GeV/c^2. The result of the study is reported in Table I. In the final fit, we fix the yield of the same-sign $B\overline{B}$ peaking background to the sum of charmless and open-charm events. The opposite-sign background in the final event sample is assumed to be negligible.

The overall reconstruction efficiency for signal events is $(9.6 \pm 0.1)\%$ for opposite-sign signal events and $(9.5 \pm 0.1)\%$ for same-sign signal events. These numbers are equal within the uncertainty as expected. The composition of the final sample is shown in Table I.

IV. FIT PROCEDURE AND RESULTS

To measure the ratios R^+ and R^- we perform extended maximum-likelihood fits to the $m_{\rm ES}$ and $\mathcal{F}$ distributions, separately for the B^+ and B^- data samples. We write the extended likelihood functions $\mathcal{L}^\pm$ as:

$$\mathcal{L}^\pm = \frac{e^{-N'}}{N!} \cdot N'^N \cdot \prod_{j=1}^{N} f^\pm(\mathbf{x}_j \mid \theta, N') \ ,$$

$$\text{with } \ f^\pm(\mathbf{x} \mid \theta, N') = \frac{1}{N'} \left(\frac{R^\pm N_{B^\pm,\rm total}}{1+R^\pm} f^\pm_{\rm sig,os}(\mathbf{x}|\theta_{\rm sig,os}) + \right.$$

$$\left. \frac{N_{B^\pm,\rm total}}{1+R^\pm} f^\pm_{\rm sig,ss}(\mathbf{x}|\theta_{\rm sig,ss}) + \sum_i N^{\rm bkg}_{B_i} f^\pm_{B_i}(\mathbf{x}|\theta) \right) ;$$

where $f_{\rm sig,ss}(\mathbf{x}|\theta_{\rm sig,ss})$, $f_{\rm sig,os}(\mathbf{x}|\theta_{\rm sig,os})$, and $f_{B_i}(\mathbf{x}|\theta)$ are the probability density functions (PDFs) of the hypotheses that the event is a same-sign signal, opposite-sign signal, or a background event (B_i are the different background categories used in the fit), respectively, N is the number of events in the selected sample, and N' is the expectation value for the total number of events. The symbol θ indicates the set of parameters to be fitted. $N_{B^\pm,\rm total}$ is the total number of signal events, $R^\pm = \frac{N_{\rm sig,os}}{N_{\rm sig,ss}}$ for the decays of the $B^\pm$ meson, and $N^{\rm bkg}_{B_i}$ is the total number of events of each background component. For the opposite-sign events the background comes from continuum and $B\overline{B}$ events. The peaking $B\overline{B}$ background is introduced as a separate component in the fit to the same-sign sample. The fit is performed to the B^+ sample (consisting of 15706 events) to determine R^+ and to the B^- sample (consisting of 15057 events) to determine R^-. The PDFs for R^+ and R^- fits are identical. The $R_{\rm ADS}$ ratio is fitted to the same likelihood ansatz, but to the combined B^+ and B^- data sample.

Since the correlations among the variables are negligible, we write the PDFs as products of the one-dimensional distributions of $m_{\rm ES}$ and $\mathcal{F}$. The absence of correlation between these distributions is checked using MC samples. The signal $m_{\rm ES}$ distributions is modeled with the same asymmetric Gaussian function for both same-sign and opposite-sign events, while the $\mathcal{F}$ distribution is taken as a sum of two Gaussians. The continuum background $m_{\rm ES}$ distributions for the same and opposite-sign events are modeled with two different threshold ARGUS functions [23] defined as follows:

$$A(x) = x\sqrt{1-\left(\frac{x}{x_0}\right)^2} \cdot e^{c\left(1-\left(\frac{x}{x_0}\right)^2\right)}, \qquad (10)$$

where x_0 represents the maximum allowed value for the variable x, and c determines the shape of the distribution. The $m_{\rm ES}$ distribution of the non-peaking $B\overline{B}$ background components are modeled with Crystal Ball (CB) functions that are different for same-sign and opposite-sign events [24]. The CB function is a Gaussian modified to include a power-law tail on the low side of the peak. The $\mathcal{F}$ distributions for the $B\overline{B}$ background are approximated with sums of two asymmetric Gaussians. For the peaking $B\overline{B}$ background we conservatively use the same parameter set as for the signal.

The PDF parameters are derived from data when possible. The parameters for continuum events are determined from the off-resonance data sample. The parameters for the $m_{\rm ES}$ distribution of signal events are extracted from the sample of $B^+ \to D\pi^+$ with $D \to K^+\pi^-\pi^0$, while for the parameters of the signal Fisher PDF we use the MC sample. The parameters of non-peaking $B\overline{B}$ distributions are determined from the MC sample.

From each fit, we extract the ratios R^+, R^-, or $R_{\rm ADS}$, the total number of signal events in the sample ($N_{B^\pm,\rm tot}$) along with the non-peaking background yields and threshold function slope for the continuum background. We fix the number of peaking $B\overline{B}$ background events.

To test the fitting procedure we generated 10000 pseudo-experiments based on the PDFs described above. The fitting procedure is then tested on these samples. We find no bias in the number of fitted events for any component of the fit. Tests of the fit procedure performed on the full MC samples give values for the yields compatible with those expected.

The main results of the fit to the data are summarized in Table II.

The fits to the $m_{\rm ES}$ for $\mathcal{F} > 0.5$ and the $\mathcal{F}$ distribution with $m_{\rm ES} > 5.27$ GeV/c^2 are shown in Fig. 2, for the combined B^+ and B^- sample. These restrictions reduce the background and retain most of the signal events. Fig. 3 shows the fits for the separate B^+ and B^- samples.

V. SYSTEMATIC UNCERTAINTIES

We consider various sources of systematic uncertainties, listed in Table III. One of the largest contributions comes from the uncertainties on the PDF parameters. To evaluate the contributions related to the $m_{\rm ES}$ and $\mathcal{F}$ PDFs, we repeat the fit varying the PDF parameters for each fit species within their statistical errors, taking into account correlations among the parameters (labeled as "PDF error" in Table III).

TABLE I: Composition of the final selected sample as evaluated from the MC samples normalized to data and from data for the charmless peaking background. The signal contribution is estimated using values of branching fractions from the PDG [9] and $r_B = 0.1$ [10]. The errors are from the statistics of the control samples only.

Sample	Region	Signal	$B\overline{B}$ non-peaking	Continuum	$D\pi$	Charmless peaking
Same sign	Fit	2252 ± 20	459 ± 12	7403 ± 62	176 ± 14	28 ± 14
	Signal	1921 ± 18	147 ± 8	203 ± 10	130 ± 14	21 ± 14
Opposite sign	Fit	28.7 ± 0.2	434 ± 12	21201 ± 104	-	-2 ± 9
	Signal	24.4 ± 0.2	65 ± 5	612 ± 18	-	-2 ± 9

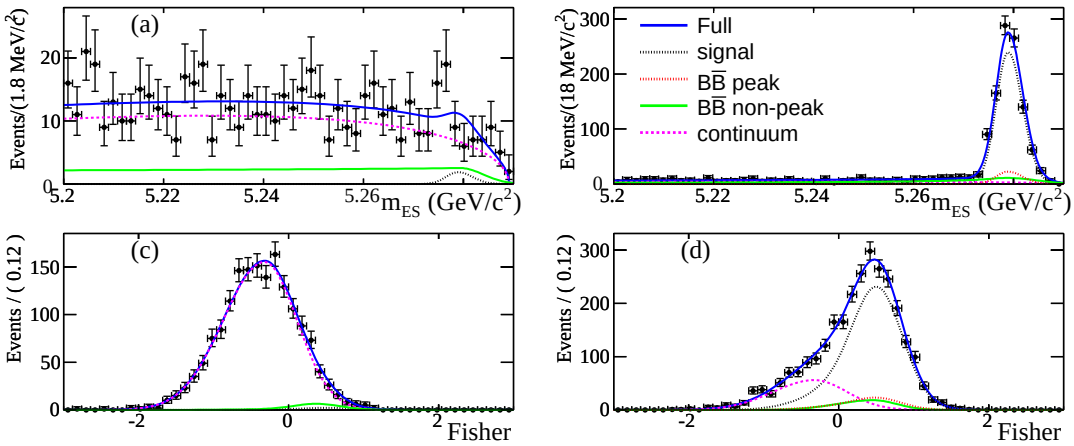

FIG. 2: (color online) Distribution of (a,b) $m_{\rm ES}$ (with $\mathcal{F} > 0.5$) and (c,d) $\mathcal{F}$ (with $m_{\rm ES} > 5.27$ GeV/c^2) and the results of the maximum likelihood fits for the combined B^+ and B^- samples (extracting $R_{\rm ADS}$), for (a,c) opposite-sign and (b,d) same-sign decays. The data are well described by the overall fit result (solid blue line) which is the sum of the signal, continuum, non-peaking, and peaking $B\overline{B}$ backgrounds.

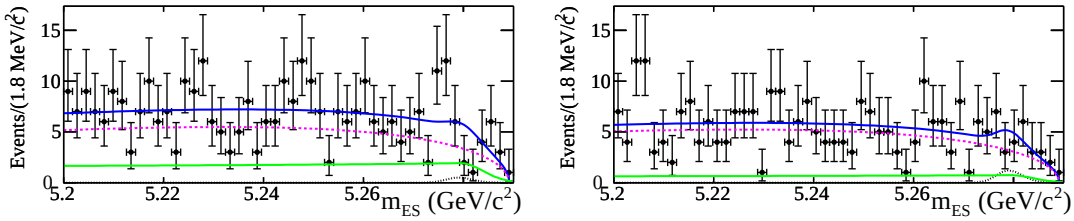

FIG. 3: (color online) Projections of the 2D likelihood for $m_{\rm ES}$ with the additional requirement $\mathcal{F} > 0.5$, obtained from the fit to the B^+ (left) and B^- (right) data sample for opposite-sign events (extracting R^+ and R^-). The labeling of the curves is the same as in Fig. 2.

To evaluate the uncertainties arising from peaking background contributions, we repeat the fit varying the the peaking $B\overline{B}$ background contribution within its statistical uncertainties and the errors of branching fractions, $\mathcal{B}$, used to estimate the contribution. For the opposite-sign events only the positive part of the probability distribution is used in the evaluation.

Differences between data and MC (labeled as "Simulation" in Table III) in the shape of the $\mathcal{F}$ distribution are studied for signal components using the data control samples of $B^+ \to D\pi^+$ with $D \to K^+\pi^-\pi^0$. These parameters are expected to be slightly different between the $B \to D\pi$ and $B \to DK$ samples. We conservatively take the systematic uncertainty as the difference in the fit results from the nominal parameters set (using MC events) and the parameters set obtained using the $B \to D\pi$ data sample.

The systematic uncertainty attributed to the cross-feed between opposite-sign and same-sign events has been evaluated from the MC samples. The number of same-sign events passing the selection of the opposite-sign events is taken as a systematic uncertainty. The efficien-

TABLE II: Results of fits to the B^+, B^-, and the combined B^+ and B^- samples, including the extracted number of signal and background events and their statistical errors.

Sample	B^+	B^-	B^+ and B^-
R, 10^{-3}	5^{+12}_{-10}	12^{+12}_{-10}	$9.1^{+8.2}_{-7.6}$
$N_{B^\pm,\mathrm{tot}}$	1032 ± 41	946 ± 39	1981 ± 57
$N^{\mathrm{bkg}}_{B\overline{B},\mathrm{OS}}$	305 ± 52	120 ± 36	402 ± 65
$N^{\mathrm{bkg}}_{B\overline{B},\mathrm{SS}}$	315 ± 44	329 ± 44	644 ± 62
$N^{\mathrm{bkg}}_{\mathrm{cont},\mathrm{OS}}$	10290 ± 111	10017 ± 105	20329 ± 154
$N^{\mathrm{bkg}}_{\mathrm{cont},\mathrm{SS}}$	3660 ± 69	3539 ± 68	7203 ± 76

TABLE III: Systematic errors for $R^\pm$ and R_{ADS} in units of 10^{-3}.

Source	R^+	R^-	R_{ADS}
PDF error	$^{+1.1}_{-1.8}$	1.1	1.0
Same sign peaking background	0.2	0.5	0.2
Opposite sign peaking background	$^{+0}_{-3.6}$	$^{+0}_{-3.6}$	$^{+0}_{-3.4}$
Simulation	0.6	0.6	0.7
$\mathcal{B}$ errors	0.2	0.6	0.4
Crossfeed contribution	0.1	0.4	0.3
Efficiency ratio	0.1	0.4	0.3
Combined uncertainty	$^{+1.2}_{-4.1}$	$^{+1.6}_{-3.9}$	$^{+1.4}_{-3.7}$

cies for same-sign and opposite-sign events were verified to be the same within a precision of 3% [25]. We hence assign a systematic uncertainty on $R^\pm$ based on variations due to changes in the efficiency ratio by $\pm 3\%$.

The systematic uncertainties for the ratios R^+, R^-, and R_{ADS} are summarized in Table III. The overall systematic errors represent the sum in quadrature of the individual uncertainties.

VI. EXTRACTION OF r_B

Following a Bayesian approach [26], the probability distributions for the R^+ and R^- ratios obtained in the fit are translated into a probability distribution for r_B using Eqs. 8 and 9 simultaneously. We assume the following prior probability distributions: for r_D a Gaussian with mean 4.7×10^{-2} and standard deviation 3×10^{-3} [9]; for k_D and δ_D, we use the likelihood obtained in Ref. [8], taking into account a 180 degree difference in the phase convention for δ_D; for γ and δ_B we assume a uniform distribution between 0 and 360 degrees, while for r_B a uniform distribution in the range $[0,1]$ is used. We obtain the posterior probability distribution shown in Fig. 4. Since the measurements are not statistically significant, we integrate over the positive portion of that distribution and obtain the upper limit $r_B < 0.13$ at 90% probability, and the range

$$r_B \in [0.01, 0.11] \text{ at } 68\% \text{ probability}, \tag{11}$$

and 0.078 as the most probable value.

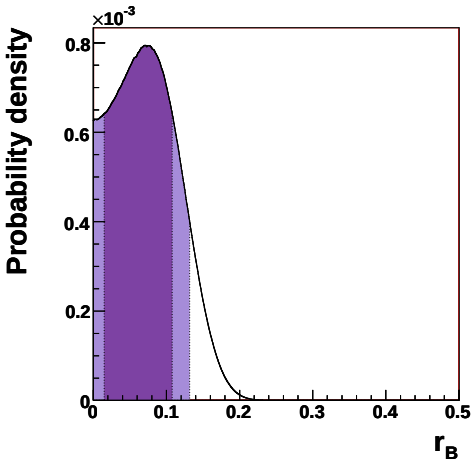

FIG. 4: Bayesian posterior probability density function for r_B from our measurement of R^+ and R^- and the hadronic D decay parameters r_D, δ_D, and k_D taken from [8] and [9]. The dark and light shaded zones represent the 68% and 90% probability regions, respectively.

VII. SUMMARY

We have presented a study of the decays $B^\pm \to D^0 K^\pm$ and $B^\pm \to \overline{D}^0 K^\pm$, in which the D^0 and $\overline{D}^0$ mesons decay to the $K^\mp\pi^\pm\pi^0$ final state using the ADS method. The analysis is performed using 474×10^6 $B\overline{B}$ pairs, the full *BABAR* dataset. Previous results [7] are improved and superseded by improved event reconstruction algorithms and analysis strategies employed on a larger data sample.

The final results are:

$$R^+ = \left(5^{+12}_{-10}(\mathrm{stat})^{+1}_{-4}(\mathrm{syst})\right)\times10^{-3}, \tag{12}$$

$$R^- = \left(12^{+12}_{-10}(\mathrm{stat})^{+2}_{-4}(\mathrm{syst})\right)\times10^{-3}, \tag{13}$$

$$R_{\mathrm{ADS}} = \left(9.1^{+8.2}_{-7.6}(\mathrm{stat})^{+1.4}_{-3.7}(\mathrm{syst})\right)\times10^{-3}, \tag{14}$$

from which we obtain 90% probability limits:

$$R^+ < 23\times10^{-3}, \tag{15}$$

$$R^- < 29\times10^{-3}, \tag{16}$$

$$R_{\mathrm{ADS}} < 21\times10^{-3}. \tag{17}$$

From our measurements we derive the limit

$$r_B < 0.13 \text{ at } 90\% \text{ probability}. \tag{18}$$

VIII. ACKNOWLEDGMENTS

We are grateful for the extraordinary contributions of our PEP-II colleagues in achieving the excellent luminosity and machine conditions that have made this work possible. The success of this project also relies critically on the expertise and dedication of the computing organizations that support *BABAR*. The collaborating institutions wish to thank SLAC for its support and the kind hospitality extended to them. This work is supported by the US Department of Energy and National Science Foundation, the Natural Sciences and Engineering Research Council (Canada), the Commissariat à l'Energie Atomique and Institut National de Physique Nucléaire et de Physique des Particules (France), the Bundesministerium für Bildung und Forschung and Deutsche Forschungsgemeinschaft (Germany), the Istituto Nazionale di Fisica Nucleare (Italy), the Foundation for Fundamental Research on Matter (The Netherlands), the Research Council of Norway, the Ministry of Education and Science of the Russian Federation, Ministerio de Ciencia e Innovación (Spain), and the Science and Technology Facilities Council (United Kingdom). Individuals have received support from the Marie-Curie IEF program (European Union), the A. P. Sloan Foundation (USA) and the Binational Science Foundation (USA-Israel).

[1] N. Cabibbo, Phys. Rev. Lett. **10** 531 (1963); M. Kobayashi and T. Maskawa, Prog. Theor. Phys. **49** 652 (1973).
[2] L. Wolfenstein, Phys. Rev. Lett. **51**, 1945 (1983).
[3] M. Gronau and D. London, Phys. Lett. **B253**, 483 (1991); M. Gronau and D. Wyler, Phys. Lett. **B265**, 172 (1991).
[4] I. Dunietz, Phys. Lett. **B270**, 75 (1991); I. Dunietz, Z. Phys. **C56**, 129 (1992); D. Atwood, G. Eilam, M. Gronau, and A. Soni, Phys. Lett. **B341**, 372 (1995); D. Atwood, I. Dunietz and A. Soni, Phys. Rev. Lett. **78**, 3257 (1997).
[5] A. Giri, Yu. Grossman, A. Soffer, and J. Zupan, Phys. Rev. **D68**, 054018 (2003).
[6] Charge conjugate processes are assumed throughout the paper.
[7] B. Aubert *et al.* (*BABAR* Collaboration), Phys. Rev. D**76**, 111101 (2007).
[8] N. Lowrey et al. (CLEO Collaboration), Phys. Rev. D **80**, 031105(R) (2009).
[9] K. Nakamura *et al.* (Particle Data Group), J. Phys. G 37, 075021 (2010).
[10] M. Bona *et al.* (UTfit Collaboration), JHEP **0507**, 028 (2005). Updated results available at `http://www.utfit.org/`.
[11] P. del Amo Sanchez *et al.* (*BABAR* Collaboration), Phys. Rev. D **82**, 072004 (2010).
[12] P. del Amo Sanchez *et al.* (*BABAR* Collaboration), Phys. Rev. D **82**, 072006 (2010).
[13] P. del Amo Sanchez *et al.* (*BABAR* Collaboration), Phys. Rev. Lett. **105**, 121801 (2010).
[14] K. Abe *et al.* (Belle Collaboration), Phys. Rev. D **73** 051106 (2006).
[15] Y. Horii *et al.* (Belle Collaboration), [arXiv:1103.5951].
[16] A. Poluektov *et al.* (Belle Collaboration), Phys. Rev. D **81**, 112002 (2010).
[17] T. Aaltonen *et al.* (CDF Collaboration), Phys. Rev. D **81**, 031105 (2010).
[18] B. Aubert *et al.* (*BABAR* Collaboration), Nucl. Instr. Methods **A479**, 1 (2002).
[19] S. Agostinelli *et al.* (GEANT4 Collaboration), Nucl. Instrum. Meth. A **506**, 250 (2003).
[20] D. J. Lange, Nucl. Instrum. Meth. A **462**, 152 (2001).
[21] T. Sjostrand, Comput. Phys. Commun. **82**, 74 (1994).
[22] B. Aubert *et al.* (*BABAR* Collaboration), Phys. Rev. D **66**, 032003 (2002).
[23] H. Albrecht *et al.* (ARGUS Collaboration), Z. Phys. **C48**, 543 (1990).
[24] M. J. Oreglia, Ph.D. Thesis, SLAC-236(1980), Appendix D; J. E. Gaiser, Ph.D Thesis, SLAC-255(1982), Appendix F; T. Skwarnicki, Ph.D Thesis, DESY F31-86-02(1986), Appendix E.
[25] B. Aubert *et al.* (*BABAR* Collaboration], Phys. Rev. D **80**, 031102 (2009).
[26] G. D'Agostini, CERN Report 99 − 03; G. D'Agostini and M. Raso, arXiv:hep-ex/0002056.